Nanostructure Evolution During Cluster Growth: Ag on H-Terminated Si(111) Surfaces

J. M. Zuo* and B. Q. Li

Department of Materials Science and Engineering and Materials Research Laboratory, University of Illinois at Urbana and Champaign, 1304 West Green Street, Urbana, Illinois 61801

(Received 21 November 2001; published 7 June 2002)

The size of small clusters has a large effect on cluster growth and structure. Using Ag clusters of sizes from ~1 to 10 nm grown on H-Si(111), we found that the cluster structure evolves in stages showing (1) irregular shapes at coverage ≤1 ML (monolayer), (2) mostly single crystal of faceted-hut-like shapes from 2 to 5 ML, and (3) defective disklike islands above 5 ML. We show that the rapid coalescence of small clusters drives the nanostructure transition and leads to a steplike growth of nanoclusters that is different from the predictions of scaling theory.

DOI: 10.1103/PhysRevLett.88.255502 PACS numbers: 81.07.–b, 61.14.–x, 68.37.Lp, 68.55.Ac

How atoms aggregate on a crystalline surface and how clusters evolve have important implications in energy- and environment-related catalytic processes and thin film growth. Internal structure of preformed nanoclusters by cluster deposition or chemical routes has long been studied by high-resolution electron microscopy [1,2]. For clusters grown on crystalline substrates, size-dependent cluster morphology has received much attention recently in Ge quantum dots [3,4]. Shape transformation is found to have a large effect on growth. For an example, Ross *et al.* show that the shape transition of strained Ge island results in a bifurcation of the cluster size distribution [4]. For epitaxial metallic clusters, the equilibrium shapes are determined by the surface and interface energies. Metallic cluster morphology and evolution of Volmer-Weber growth have been studied extensively by STM/AFM [5] and earlier by SEM and TEM [6]. With few exceptions [7], it is generally believed that growth of clusters follows scaling laws such as the size $R(t) \sim t^{x}$ and density $N(t) \sim t^{-x'}$ [8]. Here we show that in the small size regime these scaling laws are not followed. Small Ag clusters grow on H-Si(111) surfaces in stages of coalescence and growth with each stage marked by changes in the nanostructure of clusters, which includes the 3D shape, size, and defects.

We use Ag/H-Si(111) as a model system for studying cluster growth. Ag/H-Si(111) is interesting because Ag/Si is a "prototypical nonreactive" system; Ag and Si have a high eutectic temperature of 837 °C. Cluster growth is common for metals on oxide substrates or surfaces like graphite with molecular bonding. On higher energy surfaces, such as clean Si, a wetting layer typically forms at the initial stages of growth. By hydrogen passivation, we reduce both the surface and the interface energies and promote cluster growth. H-Si(111) has the ideal hexagonal (1×1) surface structure, which, prepared by chemical techniques, is very stable [9,10]. Previous studies show that Ag grows on H-Si(111) in the Volmer-Weber mode with a [111] preferred orientation [11,12]. In comparison, growth of Ag on a UHV prepared clean Si(111)-(7×7) surface follows the Stranski-Krastanov growth with a 2D wetting layer of $\sqrt{3} \times \sqrt{3}$ reconstruction [13]. No such layer was found on H-Si(111) surfaces. Hydrogen also remains at the Ag/Si interface even at the later stage of growth [12].

In situ synthesis and diffraction characterization and *ex situ* electron imaging were used for this study. *In situ* experiments were carried out in a modified UHV transmission electron microscope (for details see Ref. [14]). The sample is a 6×15 mm^2 sized Si(111) wafer (Boron-doped, $\rho \sim 10\ \Omega$ cm). It is back-thinned initially by mechanical grinding, followed by chemical etching, degreasing, and chemical cleaning for electron transparency. The top surface (growing surface) was protected by wax during etching. The final step involves etching in a 40% NH_4F solution for 10 min and a short rise in deionized water. *Ex situ* XPS, RHEED, and AFM were used to characterize the surface morphology and composition. The surface is free of contaminants and has an rms surface roughness of ~1.5 Å. The prepared substrate is then transferred to the UHV TEM. The base pressure in the sample region is $\sim 2 \times 10^{-10}$ Torr, and pressure during growth was $< 2 \times 10^{-9}$ Torr. Ag was deposited using the electron-beam evaporation at RT. The growth rate was 0.008 ML (monolayer)/s (calibrated by *in situ* Auger spectroscopy and *ex situ* Rutherford backscattering). *Ex situ* high-resolution TEM observation was made immediately after removal from the UHV TEM. All samples were prethinned in the plane-view geometry. *Ex situ* electron microscopy was done using the Phillips CM12 TEM and JEOL 2010F electron microscopes. We checked the sample transfer effect by comparing electron diffraction patterns taken before and after transfer [15]. Notably, no evidence of Ag cluster and silicon surface oxidation was found.

Figure 1 shows the structure and morphological evolution of Ag clusters at 1, 2, 5, and 10 bulk-equivalent ML. Nanometer-sized Ag clusters grow as "droplets," with the similar round faceted shapes in projection and size distributions from 2 to 10 ML coverage. At higher coverage, irregular shaped, or "stringy," Ag islands are formed that are very similar to the percolative growth by coalescence observed in many metal films grown on insulating or

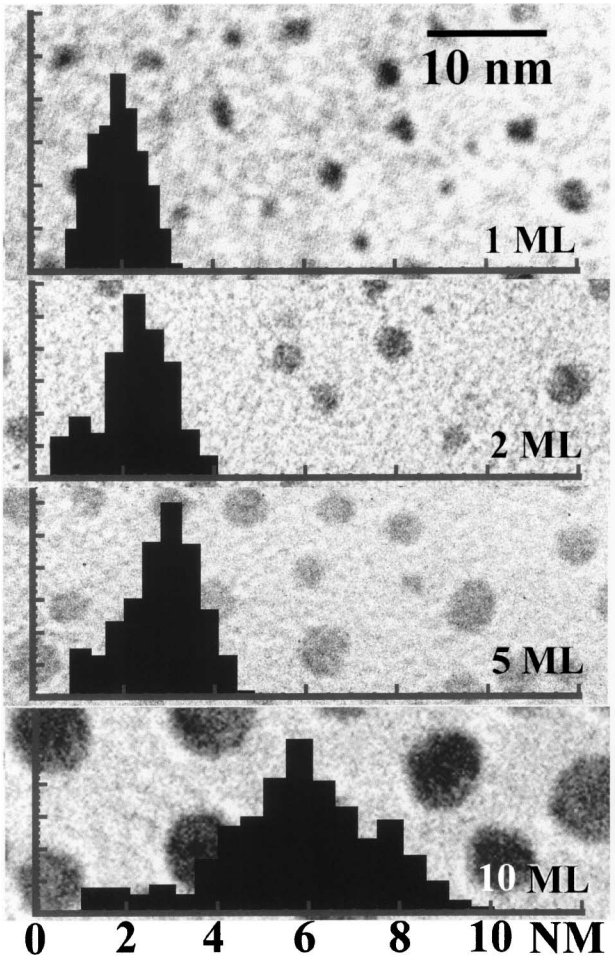

FIG. 1. Electron microscopy images and the size distributions of Ag clusters recorded and measured for 1, 2, 5, and 10 bulk-equivalent monolayer (ML) coverage. Ag appears dark from the strong scattering and a slight underfocus. The size measured is the diameter of clusters (nm) in projection. At 1 ML, Ag clusters have the irregular and angled shapes. Between 2 to 10 ML, Ag clusters are round faceted with the appearance of a droplet. The spatial distribution of clusters are random; clusters are separated by an exclusion zone.

amorphous substrates [16]. Cluster formation at 1 ML coverage is consistent with the VW growth reported previously [12]. The micrographs were taken near the [111] zone axis using the transmitted electron beam. Ag clusters appear in dark contrast due to its larger atomic scattering factor and the underfocused condition. The clusters were measured with a cutoff diameter of 0.5 nm. A cluster of 0.58 nm could have 16 or more atoms. Under our observation conditions, a cluster of this size gives a signal $\sim$2–3 times the background noise (the best sensitivity in electron microscopy is a single atom [17]). All measurements were done by processing the digital electron images recorded on a CCD camera.

The cluster density and the average 2D cluster size are plotted in Fig. 2 as a function of Ag coverage and the percentage of substrate surface area covered by clusters ε^2 (%). What is most remarkable from this figure is the step-

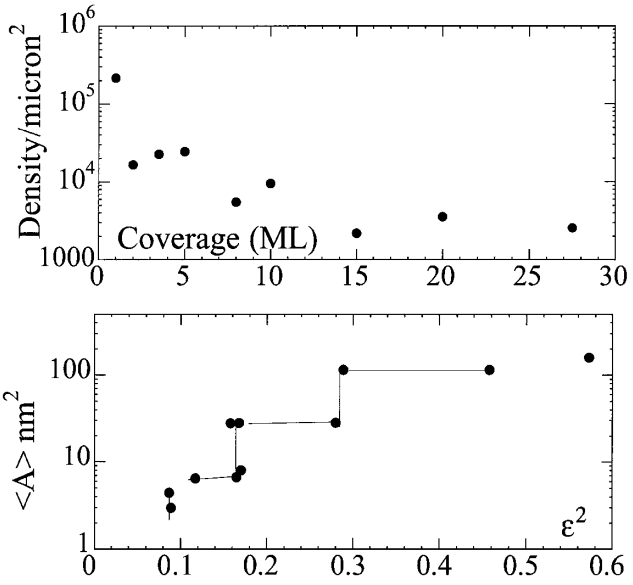

FIG. 2. (top) Area density of Ag clusters versus ML coverage (bottom) the average projected cluster area, $\langle A \rangle$, as the function of substrate surface area coverage ε^2 (% area covered by clusters). Lines are drawn for visual guidance. The three vertical lines are from 1 to 2, 5 to 8, and 10 to 15 ML. Each is associated with a drop in the cluster area density, which indicates cluster coalescence. Between coalescence, the increase in ε^2 comes mostly from the increase in the cluster density. Both figures represent deviations from the predictions of the scaling theory of self-similar growth.

like dependence of the average projected cluster area, $\langle A \rangle$ (Fig. 2b). This steplike dependence correlates with sudden drops in the cluster density (Fig. 2a). At $\varepsilon^2 = 0.09$ and 0.17, the cluster density reduces by 23% and 74.5%, respectively. Meanwhile, the number of clusters increases by approximately 47% from $\varepsilon^2 \sim 0.09$ to 0.17, and 74% from $\varepsilon^2 = 0.17$ to 0.3. Thus, there are two distinct mechanisms of Ag cluster growth. One is nucleation and growth. As the number of clusters and size increase, this growth is interrupted by coalescence. The growth during the nucleation/growth stage can be described by the power law $\langle R \rangle \sim t^n$ with $n = 0.24$ from 2 to 5 ML coverage. The polydispersity of the droplet size $g = \Delta R/\langle R \rangle$ (with R the projected radii) is nearly constant at $\sim$0.3 before and after coalescence.

The growth shown in Fig. 2 is reminiscent of the wiping and growth of breath figures studied by Beysens and Knobler [18]. For water droplets, steplike increases with time were observed for the diameter of a single droplet from coalescence. Between coalescence, the droplet grows by the power law $R \sim t^{0.23}$. The surface coverage ε^2 remains constant.

The difference between a water droplet and Ag cluster is the crystallinity, which is reflected in the growth. The steplike growth behavior is associated with distinctive cluster nanostrucutres. From 1 to 2 ML, the change from the triangular and rectangular projected shapes to the more rounded shape is visible in Fig. 1. Above 10 ML,

continuous cluster coalescence produces elongated clusters with fractal shapes. From 2 to 10 ML, the change is mostly 3D. To "see" this, we used electron weak phase imaging by placing a small objective aperture on the direct beam under slight defocus [19]. Under such a condition, it has been shown that the image intensity relates directly to the projected potential $\phi_p(x, y)$ [17]:

$$I(x, y) \approx 1 + 2\sigma\phi_p(-x, -y) * F\{\sin\chi(u, v)P(u, v)\} \quad (1)$$

with $*$ for convolution. The function $F\{\sin\chi(u, v)P(u, v)\}$ is sharply negative with a half-width $\sim$4 Å under our experimental conditions. To ensure the weak phase condition and simplify the shape measurements, we tilted the crystal $\sim$5° away from the [111] zone axis sufficiently to avoid strong dynamic diffraction. At this orientation the projected potential equal the mean potential times the thickness: $\phi_p(x, y) = V_0 t$. Additionally, we used the face-down geometry with Ag clusters on the exit-wave side of Si substrates to minimize the scattering effect of Si. Figures 3a and 3b show two of such images at the 2 and 8 ML coverage. At 2 ML, most clusters appear to be faceted (see Fig. 3c) and "hut"-like shaped, while most clusters are disklike at 8 ML. Further deposition leads to larger, mostly flat, islands.

The transition from the hut to disklike shapes is accompanied by an increasing number of clusters with defects. Figure 4 shows the examples of lattice images and the moiré fringes of Ag nanoclusters on Si(111) at the 3.5 and 8 ML coverage. At 3.5 ML, most clusters show a single set of moiré fringes, while clusters at 8 ML appear to be multiple twinned with the moiré fringes showing for only part of the cluster. Previously, multiple twinned clusters were observed in small gold particles deposited on amorphous carbon films [20]. These clusters often change shapes under electron-beam radiation. In comparison, the epitaxial Ag clusters observed here are stable. We also noticed that some clusters have a large angle between the Ag moiré and Si lattice fringes showing azimuthal misorientation. This observation here is consistent with the previous LEED study [12]. Electron diffraction measurement showed that the distribution of the azimuthal orientation is 9° at 5 to 10 ML coverage. The azimuthal orientation improves as clusters grow.

Compared to Ge on Si(100), the strain effect on Ag nanoclusters is small. Quantitative measurement by selected area electron diffraction using Si as the reference shows that the Ag nanoclusters have an average lattice constant of 4.090 $\pm$ 0.013 Å, which changes little with coverage. For bulk Ag, $a = 4.086$ Å. The ratio of the moiré fringe spacing and Si(111) lattice is 3 for clusters with the exact Ag[110] $\parallel$ Si[110] orientational epitaxy (see Fig. 4). This gives $a_{\mathrm{Ag}} = 4.073$ Å and a strain of 0.32%. Moiré fringes give a better measurement of strain, which are known to be very sensitive. The buried interface of epitaxially oriented Ag nanoclusters has the minimum energy configuration of a 3×3 coincidence lattice, consistent with the principles outlined by Dahman for heterogeneous interfaces [21].

The experimental picture emerging here shows that the small Ag clusters undergo distinctive nanostructure transition during growth on a hexagonal crystalline substrate. The rapid increase after a sharp drop in the cluster density suggests a much slower growth rate for the large

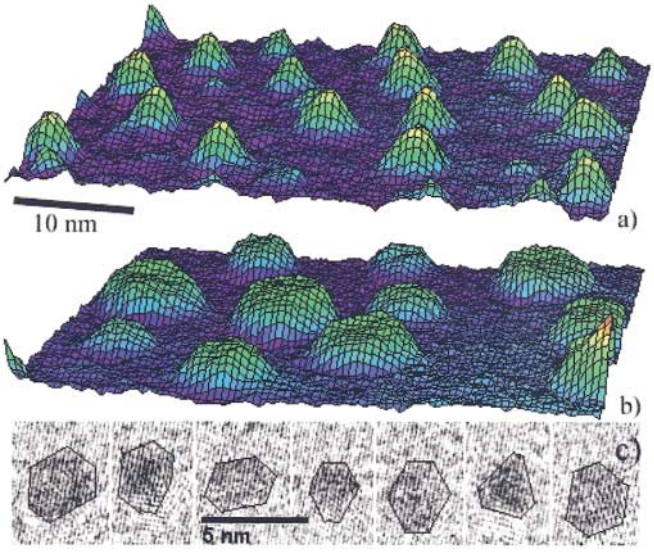

FIG. 3 (color). Surface plots of negative electron image intensities of Ag clusters at (a) 2 and (b) 8 ML coverage. The images were taken with the central beam at the off-zone axis orientation that avoids the strong dynamical scattering and is slightly underfocused. Under such conditions, small Ag clusters are weak phase objects and the image intensity is proportional to the cluster thickness. The resolution $\sim$4 Å is determined by the small objective aperture used; (c) HREM image of cluster shapes at 2 ML. The lattice fringe is from Si(220). Most of these clusters have {111} facets.

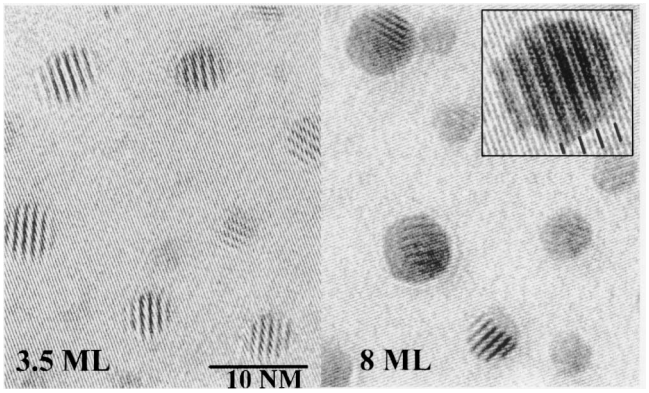

FIG. 4. Electron moiré fringes and Si(111) lattice fringes of Ag nanoclusters. At 3.5 ML, most large clusters have one set of moiré fringes (small clusters are too weak to see), while the larger clusters at 8 ML coverage show moiré fringes for only part of the cluster. The inset shows the relative spacing of moiré fringes and Si(111) lattice for an epitaxial Ag cluster.

clusters than the nucleation and growth of smaller clusters. Slow growth of large metallic clusters was previously observed for faceted Pt clusters of ~10 nm radius on Al_2O_3 under partial oxidation atmosphere by Wynblatt and Gjostein [22] and attributed to the inhibited growth by Ahn *et al.* [23]. The droplet growth can be attributed to a liquidlike rapid coalescence of small clusters. The transition from droplet to elongated island growth occurs between 10 and 15 ML with a time elapse of ~10 min. The critical diameter is ~12 nm, at which the coalescence time is larger than the time to grow a droplet. According to Nicols [24], the time for sintering two equal spheres in contact is $\propto R^4/B$. For the average cluster size of 2.8 nm at 5 ML, the coalescence time is only 0.3% of that at 15 ML. Most clusters at 15 ML appear with eliminated necks. If we take the limit of 5 min for this process, we can place an up-limit of 5 s on the average coalescence time at 5 ML at RT. The constant B is proportional to surface energy and diffusivity. Since the surface energy of Ag is comparatively small, the rapid coalescence can be attributed to the self-mobility of Ag atoms and the small size of clusters.

In conclusion, using Ag/Si(111)-H as a model system for investigating aggregation on a crystalline surface with weak forces at the nanometer scale, we show that the small Ag clusters undergo stages of liquidlike rapid coalescence alternating with nucleation and growth. Steplike growth behavior is observed, and each stage is marked by a distinctive change in the cluster shape, size, and defect structures. This deviates from the continuous time dependence of cluster density and sizes predicted by the scaling theory. The results here show the importance of coalescence in nanostructure formation and defect introduction.

This work is supported by DOE DEFG02-01ER45923 and DEFG02-91ER45439 (B. Q. L.). The authors thank Dr. M. Kleinshimdt and Dr. M. Gibson for help with the UHV electron microscope, Dr. Ray Twesten of the CMM at UIUC for the use of JEOL2010F electron microscope, and Dr. D. Cahill for comments.

*Corresponding author.
Email address: jianzuo@uiuc.edu

[1] Z. L. Wang, J. Phys. Chem. B **104**, 1153 (2000); P. L. Hansen *et al.,* Science **295**, 2053 (2002).
[2] B. Pauwels *et al.,* Phys. Rev. B **62**, 10 383 (2000); S. Iijima and T Ichihashi, Phys. Rev. Lett. **56**, 616 (1986); also Ref. [20].
[3] G. Medeiros-Ribeiro, A. M. Bratkovski, I. I. Kamins, D. A. A. Ohlberg, and R. S. Williams, Science **279**, 353 (1998).
[4] F. M. Ross, J. Tersoff, and R. M. Tromp, Phys. Rev. Lett. **80**, 984 (1998).
[5] W. W. Pai *et al.,* Phys. Rev. Lett. **79**, 3210 (1997); L. Gavioli *et al.,* Phys. Rev. Lett. **82**, 129 (1999).
[6] For examples, see D. W. Pashley, Adv. Phys. **14**, 327 (1965); K. R. Heim, S. T. Coyle, G. G. Hembree, J. A. Vanables, and M. R. Scheinfein, J. Appl. Phys. **80**, 1161 (1996).
[7] The interface electronic effect may lead to the growth of islands of uniform heights at low temperature; for an example, see V. Yeh *et al.,* Phys. Rev. Lett. **85**, 5185 (2000).
[8] The exponent x and x' depend on the type of growth; see F. Family and P. Meakin, Phys. Rev. Lett. **61**, 428 (1988); M. Zinke-Allmang, L. C. Feldman, and M. H. Grabow, Surf. Sci. Rep. **16**, 377 (1992).
[9] G. S. Higashi, Y. J. Chabal, G. W. Trucks, and K. Raghavachari, Appl. Phys. Lett. **56**, 656 (1990).
[10] Y.-C. Huang, J. Flidr, T. A. Newton, and M. A. Hines, J. Chem. Phys. **109**, 5025 (1998).
[11] K. Sumitomo *et al.,* Phys. Rev. Lett. **66**, 1193 (1991).
[12] A. Nishiyama *et al.,* Surf. Sci. **350**, 229 (1996).
[13] K. J. Wan, X. F. Lin, and J. Nogami, Phys. Rev. B **47**, 13 700 (1993).
[14] M. T. Marshall, M. L. McDonald, X. Tong, M. Yeadon, and J. M. Gibson, Rev. Sci. Instrum. **69**, 440 (1998).
[15] Two diffraction spots were used to monitor the sample: the Ag diffraction spot and the Si(422)/3 surface termination spot. The Ag spot profile gives the average size and orientation. The Si(422)/3 spot disappers when surface oxides form. No noticeable change from sample transfer was observed.
[16] About 10 ML, cluster coalescence leads to irregularly shaped island, and percolation of islands occurs at ~60 ML. Details will be published later.
[17] J. C. H. Spence, *Experimental High-Resolution Electron Microscopy* (Oxford University Press, Oxford, 1988).
[18] D. Beysens and C. M. Knobler, Phys. Rev. Lett. **57**, 1433 (1986).
[19] C. P. Liu, P. D. Miller, W. L. Henstrom, and J. M. Gibson, J. Microsc. **199**, 130 (2000).
[20] L. D. Marks, Rep. Prog. Phys. **57**, 603 (1994).
[21] U. Dahmen, Acta Metall. **30**, 63 (1982).
[22] P. Wynblatt and N. A. Gjostein, Scr. Metall. **7**, 969 (1973).
[23] T. M. Ahn, S. Purushothaman, and J. K. Tien, J. Phys. Chem. Solids **37**, 777 (1976).
[24] F. A. Nicols, J. Appl. Phys. **37**, 2805 (1966).